Evaluating Hydrodynamic and Bathtub Water-Level Models to Assess Storm Surge Flooding in Tuktoyaktuk

Daniel Pinheiro [1*], Gonçalo Vieira [1], Dustin Whalen [2], Pedro Pina [3], João Canário [4], Pedro Freitas [1] and Shawn Stuckey [5]

[1] Centre of Geographical Studies, IGOT, University of Lisbon, Lisbon, Portugal
[2] Natural Resources Canada, Dartmouth, Nova Scotia, Canada
[3] University of Coimbra, Institute of Astrophysics and Space Sciences, Department of Earth Sciences, 3030-790 Coimbra, Portugal
[4] Centre of Structural Chemistry, Instituto Superior Técnico, University of Lisbon, Lisbon, Portugal
[5] Hamlet of Tuktoyaktuk, Tuktoyaktuk, Northwest Territories, Canada; sao@tuktoyaktuk.ca

* Correspondence: Daniel Pinheiro (danielpinheiro@tecnico.pt)

Abstract: Arctic warming is leading to an increased reduction in sea ice, with models for 2100 indicating a reduction in the Arctic sea ice area from 43 to 94% in September and from 8 to 34% in February (IPCC, 2021). The increase of the sea-ice free season duration will result in more exposure of the coasts to wave action, with changing climate also modifying the contribution of terrestrial erosion processes. Coastal erosion in permafrost regions can also be enhanced by warmer seawaters and sea-level rise, with more frequent storms and associated surge events. During the short open water season (June to October) there has been an increase in coastal storms in the Beaufort Sea (wind speed > 36 km/h and surge level > 1.5m), this has led to an increment in coastal erosion and flooding (Fritz et al., 2015, Ramage et al., 2018). This work focused on the Hamlet of Tuktoyaktuk (Northwest Territories, Canada), where ultra-high-resolution surveys with unmanned aerial vehicles (UAVs) have been conducted, allowing to generate orthophoto mosaics and digital surface models (DSM) that were used as inputs for a probabilistic bathtub-like flood model and MOHID Water hydrodynamic model. The results of the probabilistic model show that using the UAV data, that has a spatial resolution of 0.1 m, translates in precise overlaps with the modelled and real water surface, reducing the overall overestimation of flooded areas obtained by using the 2004 LiDAR digital elevation model (DEM) with a 1 m spatial resolution. From the IPCC scenarios RCP4.5 and RCP8.5, respectively, it is expected that 29.2 to 32.2% of the study area is permanently submerged by 2100, only accounting for the sea level rise. These percentages can go up to 76.5 to 80% during a storm surge event with a 100-year return period.

Keywords: flood map; coastal flooding; bathtub modelling; hydrodynamic modelling; UAV; LiDAR; climate change

1. Introduction

Regions in the northern hemisphere at higher latitudes will be more affected by climate change than lower latitude regions (Räisänen, 2001). The predicted reduction in sea ice (Johannssen et al., 2002) translates in a longer period for storms to erode the coastline. According to Johannssen et al. (2002), the expected increase in temperature during summer leads to the melting of ice-bounded sediments in coastal cliffs. The Beaufort Sea coast consists of unconsolidated sediments which makes it an exceptionally dynamic environment vulnerable to marine processes such as wave action, tides, storm surges, and ice push, as well as permafrost degradation processes, such as thermo-erosion and thaw subsidence (Harper, 1990). For coastal settlements, the risk of storm-surge flooding associated with sea level rise is of major concern. Satellite data shows that the global mean sea level has been increasing at a rate of 3 ± 0.4 mm per year between January 1993 and July 2020 (NOAA, 2021), and locally, with a rate of 2.75 ± 1.07 mm per year, from 1961 to 2020, based on detrended tide gauge data (NOAA, 2021). According to the Intergovernmental Panel on Climate Change (IPCC), the mean sea level is expected to rise more than 1 m, by 2100, mainly due to thermal expansion of the oceans and increased melting of land ice (IPCC, 2021; Church et al., 2013a), leading to an increase in storm surge frequency. Tuktoyaktuk, is located in a low-lying area in the Kugmallit Bay, where severe coastal erosion destruction has been continuously documented (Solomon, 2005). The main cause of coastal erosion along the coast of Tuktoyaktuk is wind-induced storm surge events that are most frequent during late summer (Manson and Solomon, 2007). Storm surges expose the population in coastal areas to flooding and structural destruction.

Accurate and understandable forecasts, and inundation mapping products play important roles in preparing for and mitigating these events, including flood protection and evacuation. Measures to control coastal erosion in Tuktoyaktuk have been implemented over the past years but the effect of sea level rise translates in the need of continuously monitoring, maintenance and possibly, the construction of new structures to mitigate erosion. The identification of areas prone to flooding is of major interest to support climate change adaptation and mitigation before Tuktoyaktuk becomes permanently uninhabitable.

2. Study Area

The Tuktoyaktuk Peninsula (**Figure *1***) is a 40 km wide peninsula that stretches northeast for 160 km from Tuktoyaktuk to Cape Dalhousie. The peninsula lies within the zone of continuous permafrost where the thickness ranges from 200 m to over 600 m (Burn and Kokelj, 2009). It is characterized by predominant poorly drained areas that typically contain polygonal terrain and organic soils (Steedman et al., 2016). The vegetation is characterized by dwarf-shrub tundra along the whole peninsula (Timoney et al., 1992). The region is characterised by colder and drier conditions near the coast with warmer and wetter conditions inland. The mean annual air temperature for 1981-2010 at Tuktoyaktuk was -10.1 ± 1.3 ºC, a mean annual snowfall of 103.1 cm and 74.9 mm of mean annual rainfall (Environment Canada, 2021). The wind regime in Tuktoyaktuk is bimodal during late summer with higher frequencies of north-westerly and south-easterly winds (Manson and Solomon, 2007). Increasing air temperatures registered since the 1970s have been associated with an increase in permafrost temperatures (Burn and Zhang, 2010). The region is characterized by very shallow nearshore seaward slopes surrounding Tuktoyaktuk Peninsula and the Mackenzie Bay with coast-parallel isobaths and a very low gradient. Offshore sea ice is present for approximately 9 months of the year, preventing wave action and coastal processes. Sea ice re-forms annually in the Beaufort Sea, limiting the open-water season to approximately 3 months, from mid-July to mid-October. The occurrence of offshore sea ice limits wave action even during the open water season, meaning that the Beaufort Sea has significantly low wave-energy (Harper, 1990). The tide amplitude in the Beaufort Sea ranges from 0.3 m for neap tides and 0.5 m for spring tides. Storm surges caused by strong winds are frequent and surveys of log debris indicate storm surge water height of 2.4 m above mean sea level in Tuktoyaktuk (Harper et al., 1998).

The peninsula on which the Hamlet of Tuk is located is composed mostly of glaciofluvial sands, typically on of 2.0 to 3.0 m thick, and underlain by massive ground ice. The tundra landscape and near-shore sea surrounding Tuktoyaktuk are characterized by sparse but varied flora and fauna, including many species crucial to the community livelihood and diet, such as caribou, bears, muskox, fox, geese, ducks, seals, whales, and fish (Manson et al., 2005). The Inuvialuit Hamlet of Tuktoyaktuk, population 995 (Northwest Territories Bureau of Statistics, 2021), located in Tuktoyaktuk Peninsula, is the most northern community on mainland. The hamlet was formerly known as Port Brabant, and nowadays is commonly abbreviated to "Tuk". Tourism during summer provide seasonal employment to a few people, especially after the construction of the Dempster Highway in 2017 that brought Tuk closer to Inuvik and strengthened its access to the South (Community of Tuktoyaktuk, 2008). Before the construction of the Dempster Highway, Tuk was only accessed by sea, a winter road or by airplane. Tuktoyaktuk's infrastructure comprise one school, Mangilaluk School that provides education up to 12th grade, a community hall (Kitti Hall), several other recreational facilities such as a swimming pool, gymnasium, and a health centre (NWT Bureau of Statistics, 2013)

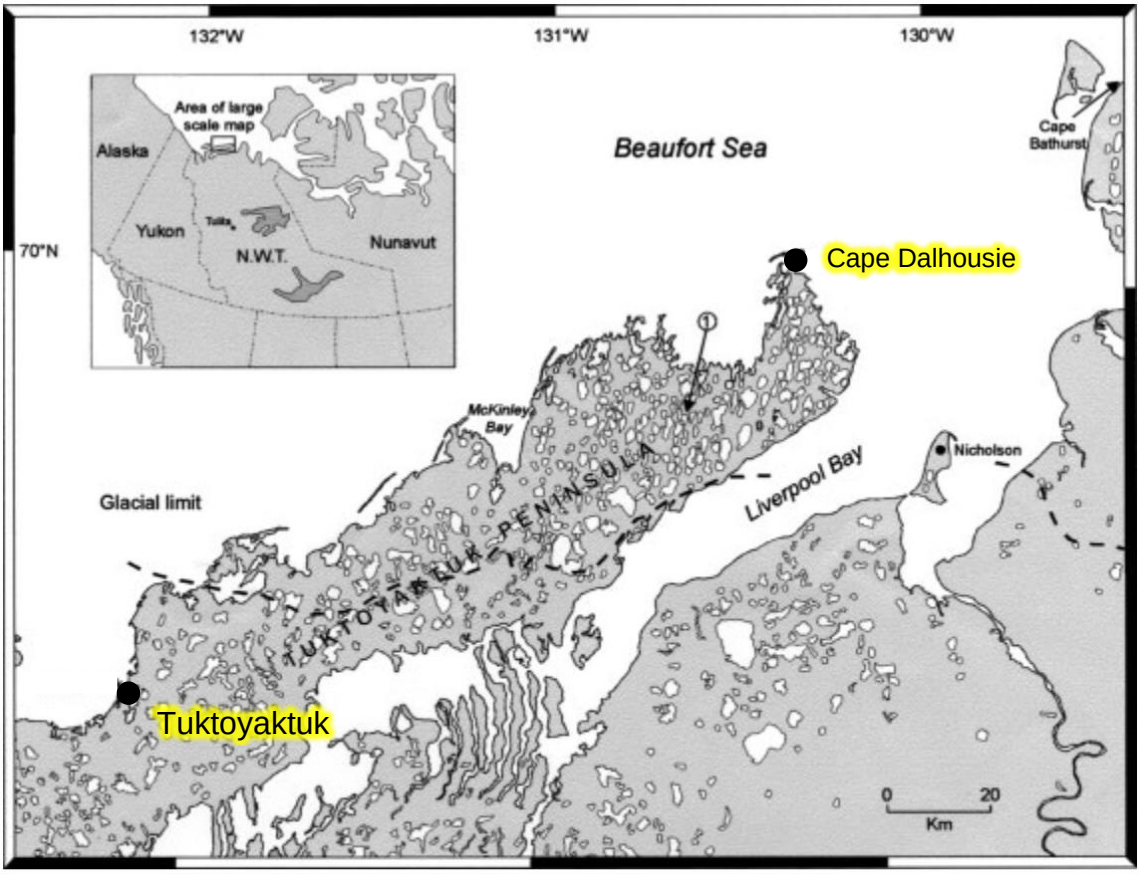

Figure 1. The Beaufort coast and Tuktoyaktuk Peninsula area (Côté and Burn, 2002).

3. Materials and Methods

3.1. Methodological Framework

Initially, to create the base data for modelling, the real time kinematic (RTK) data acquired in the field during the summer of 2019 was processed and imported to GIS. Features such as water bodies, culverts and the shoreline were digitized in ArcGIS Pro using the 2018 UAV footage and DSM and LiDAR elevation datasets added to the geodatabase. Infrastructure data was obtained from Administration of the Territorial Land Acts System (ATLAS) (Government of Northwest Territories, 2021). map viewer, a Government of Northwest Territories open geodatabase and the nautical chart used to derive bathymetry, from the Canadian Hydrographic Service. The data used for harmonics and storm surge water level analysis was gathered from Fisheries and Oceans Canada (DFO) and processed in Microsoft Excel and MATLAB. It was then combined with the IPCC local sea level rise predictions to create the simulated scenarios. The collected and processed data was used for the two modelling approaches, in ArcGIS Pro for the bathtub model, and in MOHID Studio for the hydrodynamic model MOHID Water. In a final stage, the water surface outputs from both models for the years of 2020, 2060 and 2100 were overlayed with the infrastructure data in order to identify buildings and roads affected by the different scenarios of flooding.

3.2. UAV DSM

Tuktoyaktuk's high-resolution DSM and orthophotographic maps were obtained by digital photogrammetry methods linking image matching and structure from motion (SfM) algorithms. In this study, the UAV used was a fixed wing (96 cm wingspan) eBee Plus from Sensefly. The surveys took place on the 2nd and 3rd of August 2018 where a 4.6 km2 area was covered with a spatial resolution of 10 cm/pixel. The UAV was equipped with a senseFly S.O.D.A camera with a F/2.8-11, 10.6 mm (35 mm equivalent: 29 mm) RGB lens with a resolution of 20 MP, The UAV data processing was done in Pix4D Mapper Pro using an AMD Ryzen 9 3900X 12 Core CPU with 64 GB of RAM and a Nvidia GTX 1660 Ti to perform feature detection, image matching and modelling using Pix4D's disclosed SfM algorithms. The average ground sampling distance (GSD) was 2.32 cm and the number of calibrated images 5020 out of 5955.

3.3. LiDAR DEM

In this study, the LiDAR DEM used was provided by the Geological Survey of Canada and it was surveyed in 2004 using a manned aircraft, producing a model with 1 m of spatial resolution. The DEM, defined on the Canadian Geodetic Vertical Datum of 1928 (CGVD28) was converted to the modernized vertical datum of CGVD2013, using the ArcGIS Pro transformation tool.

3.4. Flooding Data and Scenarios

3.4.1. Tide Gauge Data

The tidal records in Chart Datum (CD) for Tuktoyaktuk (**Figure 2**) were extracted from Fisheries and Oceans Canada website (DFO, 2021) and extend back only to 1961, with significant gaps between 1981 to 1991 and 1992 to 2003. The water level data was then converted to the Canadian Geodetic Vertical Datum of 2013 (CGVD2013) by corresponding the uppermost limit of the water surface on the UAV orthophoto map, the timestamp of the picture and the record by the tide gauge in 44 points along the shoreline of the study area.

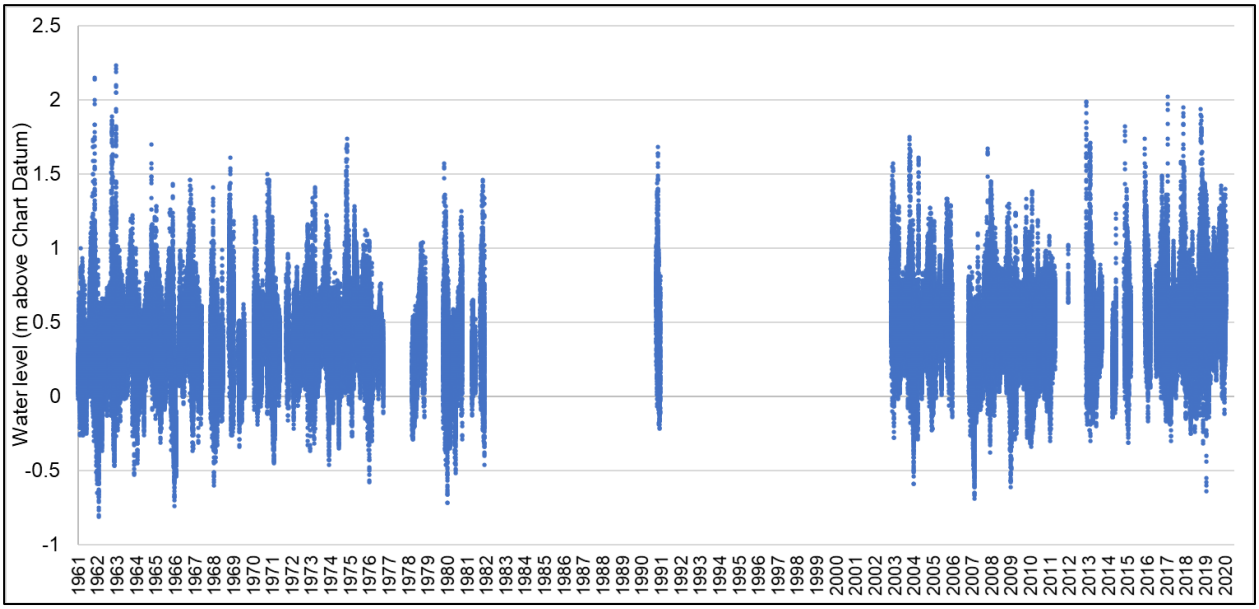

Figure 2. Open-water season hourly water level data extracted from Tuktoyaktuk tide gauge.

3.4.2. Sea Level Rise Scenarios

The selected SLR scenarios are established on the Representative Concentration Pathways (RCP) scenarios (Moss et al., 2010) as described in the Fifth Assessment Report (AR5) of the IPCC: RCP4.5 and RCP8.5. These scenarios represent different greenhouse gas concentration pathways where the number in each name corresponds to the net radiative forcing in W m-2 at 2100. The SLR data used is represented in Figure 3. It is possible to see that the average values for both RCP scenarios, and its confidence intervals starts diverging more significantly after the year 2040. In 2100, the uppermost limit of the 95% confidence interval for scenario RCP8.5 indicates a threatening sea level rise of 0.95 m surrounding Tuktoyaktuk.

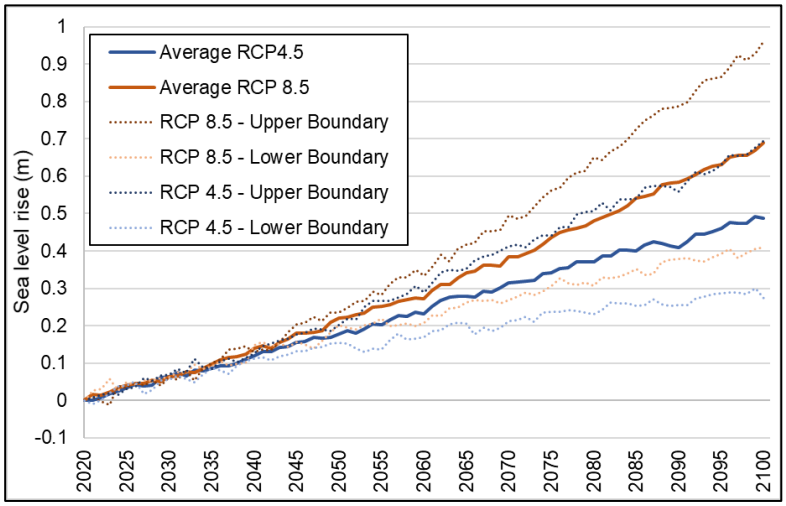

Figure 3. Predicted sea level rise based on IPCC Scenarios RCP4.5 and RCP8.5 with a confidence interval of 95% relative to 1986-2005 for Tuktoyaktuk – extracted at 70.5 N; 133.5 W from https://icdc.cen.uni-hamburg.de/las/getUI.do (Church et al., 2013).

3.1.1. Storm Surge Analysis

On top of the SLR scenarios two storm surge return periods were included in the flood analysis, a 50-year return period and a 100-year return period. To calculate the return periods, it was necessary to isolate the water level records from Tuk's tide gauge into their three components: mean sea level (MSL), astronomical tide and non-tidal residual (Pugh, 1987), by performing a harmonic analysis. For the harmonic analysis, only the years with 50% or more of completion data were used to estimate tide harmonics as suggested by Parker (2007). The software package used in MATLAB was UTide (Codiga, 2021) tool. Since the harmonic function of degree zero reflects the MSL, estimated yearly, by subtracting the modelled harmonics output from the tide gauge hourly data, the resulting non-tidal residue is detrended of the SLR (Vieira et al., 2012). This process was applied to all the available water level time series of hourly data, for the open water season, in order to extract the yearly maximum of the non-tidal residual that corresponds to the storm surge water level. The yearly maximum storm surge water level was then inputted for the extreme event analysis where a simple Gumbel distribution was used to compute flood return periods for the storm surge scenarios modelled (Al-Mashidani et al., 1978). There are reports from higher surges that are nor part of the record, with water levels of approximately 3 m above MSL and winds up to 40-50 m/s that occurred in 1944 and 1970 (Reimnitz et al., 1979), but only the tide gauge data available was used to compute the surge return periods.

3.2. Bathtub Flood Modelling

The designed bathtub model, based on NOAA's (2010) approach, produces maps that include 4 hazard probability classes (**Table 1**) by incorporating the uncertainties of SLR and storm surge projections, elevation RMSE and conversion of the water level in CD to CGVD2013. RCP 4.5 and RCP 8.5 SLR scenarios were added on top of the derived mean highest astronomical tide and for both storm surge return periods (50-year and 100-year). The hydrological connectivity of cells was set by the Region Group tool in ArcGIS Pro with eight neighbours, meaning that the connectivity is evaluated in both orthogonal and diagonal of each input. Culverts that allow the flow of water from and to areas that would be unconnected by analysing solely the elevation data, were incorporated in both elevation datasets. A third level of hydrological connectivity is related with the shoreline. Since the focus in a bathtub approach is SLR, flooding will only occur if there is connectivity to the existing water surface.

Table 1. Probability range and hazard classes used for mapping. Adapted from Antunes et al. (2019).

Hazard Class	**Low**	**Moderate**	**High**	**Extreme**
Level	2	3	4	5
Flood Probability	20–40 %	40 – 60 %	60–80 %	>80 %

3.3. Hydrodynamic Flood Modelling (MOHID)

MOHID Water is a 3D numerical model that simulates free surface water bodies developed by MARETEC (Marine and Environmental Technology Research Centre) at Instituto Superior Técnico, University of Lisbon. The model has been used in several coastal and estuarine locations and it can simulate complex features of flows (Mateus & Neves, 2013). It started with a finite-differences approach and later incorporated baroclinic mode (Santos, 1995) and finite volumes for generic vertical coordinates (Martins, 2001). The hydrodynamic model grid was set with a regular cell size of 5 x 5 m to preserve as much of the elevation data details as possible while maintaining an acceptable computing time, the tidal forcing was applied on 9 points along the north and west boundaries of the grid data. The water level used for each simulation was forced in these points to generate the tidal wave and then validated at the tide gauge location: 69°26'19.18"N, 132°59'36.51"W. Bathymetry data was derived from the nautical chart "Chart 7685 – Tuktoyaktuk Harbour and Approaches" obtained from the Canadian Hydrographic Service. The points given in height above CD with known depth were digitized manually and interpolated using the inverse distance weighted (IDW) method.

3.4. Validation

The use of the georeferenced aerial footage facilitates the process of validation due to the high number of pictures taken along the shoreline. The timestamp of each picture was used to relate the shoreline water height with the water level given by the tide gauge at the locations represented in **Figure 4**. These points were used to establish the correspondence between Chart Datum and the vertical datum of both DSM and DEM, CGVD2013, by extracting the value of Z from the UAV DSM at the uppermost limit of the water surface to compute the difference between the water level recorded at the tide gauge at the time of the picture taken by the UAV.

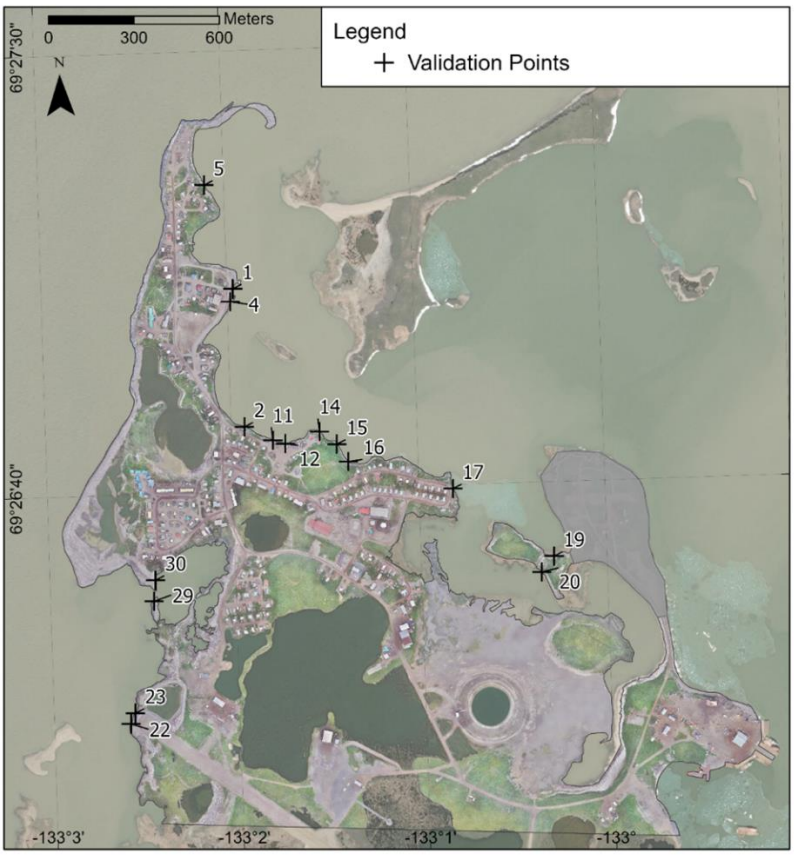

Figure 4. Location of the points used to validate the inundation models.

Traditional knowledge shared by the local community was used in the validation process of the inundation models. The information was provided in form of geodata given by the staff of the Hamlet of Tuktoyaktuk informal interviews and testimonials by locals. Several visits to the most affected areas were arranged by the Hamlet where detailed information regarding reference points from previous flood events were recorded.

4. Analysis and Discussion of the Results

4.1. Validation

The water surface simulated by the bathtub model on the LiDAR DEM shows precise positioning along the shoreline segment, even with a 1 x 1 m cell size, but the main difference resides in the flood probability classes returned by each elevation dataset. The UAV displays an almost perfect alignment with the shoreline feature, with hazard classes 5 and 4 limiting the water surface, while the LiDAR data outputs a larger flooded extent, the hazard classes range from 2 to 3 in both sides of the water-land interface. The phenomenon is verified in the majority of the points used for validation (1, 2, 4, 5, 12, 19, 20, 22, 23, 29 and 30) with hazard class 4 and 5 describing almost perfectly the shoreline, however there are exceptions where the hazard class that better describes the shoreline feature drop to 3 or even 2, that is the case of points 11, 14, 15, 16 and 17 that are all located in central sector of the study area facing north, indicating that, especially in this area, all the probability classes should definitely be considered for flood mapping. For all the points validated the LiDAR only matched the water surface with classes not higher than 3 although the simulated water surface showed an overall accuracy as depicted in Figure 43 and not exceeding 5 m further inland from the shoreline. The hydrodynamic model ran on both elevation datasets returned very similar extents across the study area. The UAV model only estimated flood extents further inland when compared to the LiDAR in the north sector of the study area, where it is known that the UAV typically shows elevation values below the LiDAR DEM. The simulated extents for the points and surrounding shoreline segments analysed did not show deviations from the shoreline polyline feature higher than 15 m for both UAV and LiDAR. In **Figure *5***, the yellow circled areas represent a small patch of vegetation that are visible in the bathtub model as hazard classes 4 and 3 on the UAV DSM. The DSM also shows increased accuracy in the centre of the road, where the results reflect the increased accuracy by the higher probability hazard classes 4 and 3, as opposed to the LiDAR's class 2. The simulation in MOHID resulted in an unconnected area (**Figure *6***) for the LiDAR DEM.

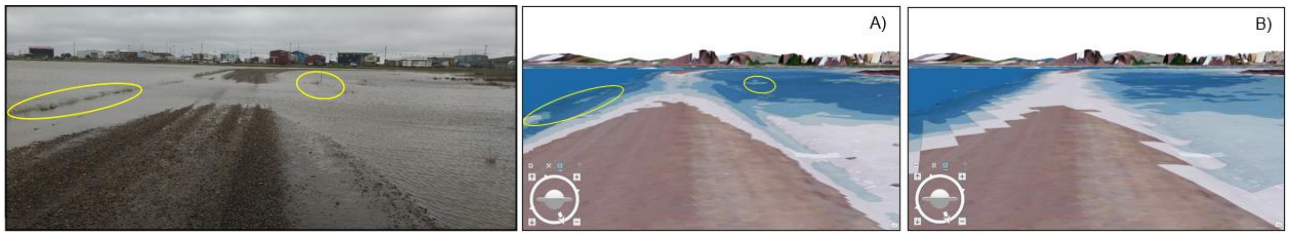

Figure 5. Storm surge event on the 5th of august 2019 at 09:47 AM (local time) with a water level of 1.39 m above Chart Datum and bathtub model output. A) UAV DSM. B) LiDAR DEM.

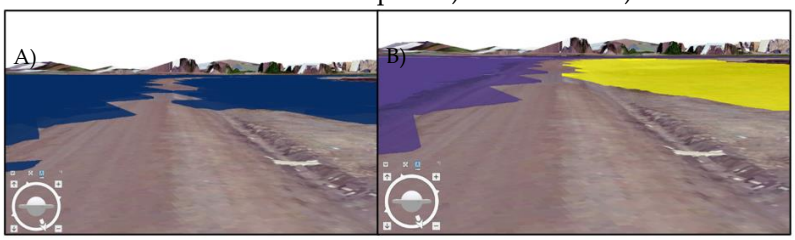

Figure 6. Storm surge event on the 5th of August 2019 at 2019 at 09:47 AM (local time) with a water level of 1.39 m above CD modelled in MOHID. A) UAV DSM. B) LiDAR DEM. The yellow polygon represents an unconnected area and not considered flooded.

4.1. Sea Level Change and Shore Line Retreat in the 21st Century

The total extent obtained by the bathtub model is higher than by MOHID for every simulation, especially for the years 2060 and 2100 because of sea level rise projections that introduce more uncertainty to the model as it increases in the inundated areas of lower probabilities by also increasing the effective water level for each different hazard class. For the year 2020, MOHID estimates that the percentage of the study area flooded is 7.7 and 9.1% for the UAV and LiDAR models respectively, while the bathtub model values are 16.3% for the UAV and 19.5% for LiDAR. In 2060, for the scenario RCP4.5, the difference between the hydrodynamic model results and the bathtub increases when compared to 2020, MOHID predicts 8.9 and 10.6% for the UAV and LiDAR, respectively, but the bathtub model outputs 22.4% for the UAV and 25.7% for the LiDAR. The same trend is visible for the RCP8.5, representing 9.3% for UAV and 11% for LiDAR in MOHID compared to the bathtub's 23.5 and 26.6 % for UAV and LiDAR, respectively. For the flooded areas predicted for the year of 2100, the same trend applies, where the hydrodynamic model (RCP4.5) returns 14,4 and 16,8%

of the study area flooded for the UAV and LiDAR, respectively, and 16,1 and 18.8% for RCP8.5. The bathtub model estimates for the scenario RCP4.5 29.2% for the UAV and 31.5% for LiDAR while the most extreme scenario represented by RCP8.5 shows that the UAV estimates 32.2% and LiDAR 35.9% of the study area as flooded. The bathtub model results for the year of 2100 for both RCP scenarios 4.5 and 8.5 are represented in **Figure 7** for the year 2100. The results of the hydrodynamic model for 2100 coincide with the uppermost limit of hazard class 3 of the bathtub model outputs for the current flooding events. This means that the estimated sea-level rise in 2100 will generate a permanent situation, at least as bad as the current flooding events, and without considering the coastal erosion effects, nor the effects of the isostatic subsidence and permafrost degradation.

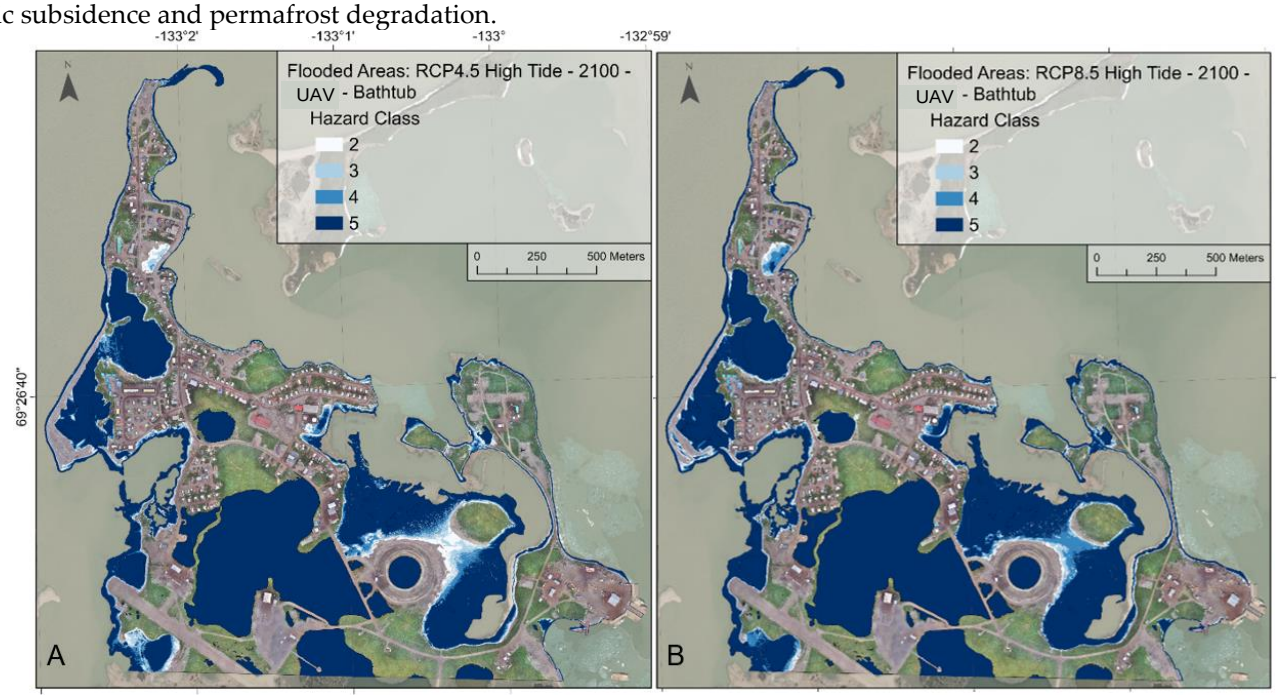

Figure 7. Bathtub model predicted highest astronomical tide for the year 2100 by hazard class on UAV DSM. A) RCP4.5. B) RCP8.5.

4.2. Storm Surge Flood Modelling in the 21st Century

4.2.1. 50-year Return Period Storm Surge Event

The total area flooded, in m2, for the 50-year return period simulations, reflects the same trend in estimating larger flood extents by both bathtub and hydrodynamic models ran on LiDAR data and smaller inundated areas calculated by MOHID compared to bathtub model. For the year 2020, MOHID, shows that 47.5% of the study area is considered flooded using the UAV and 52.3% for the LiDAR, while the bathtub model results range from 57.1 to 65.8% for the UAV and LiDAR, respectively. In 2100, with a projected sea level rise of 0.69 m for the RCP8.5 scenario, the UAV bathtub model covers 76.2% and the LiDAR 83.7% of the study area with all four hazard classes while the hydrodynamic model, shows a range from 50,6% (UAV) to 59.4% (LiDAR) which correspond approximately to the bathtub model's classes of 4 and 5 combined. The year 2020, as stated in chapter 5.5, does not resemble any RCP scenario since it represents the highest astronomical tide added to the mean sea level and the 50-year return period storm surge water level of 1.9 m. The differences between the LiDAR and the UAV partially reside in the fact that the LiDAR does not include features such as buildings, sheds and sizeable containers used as storage units or even cars and boats that are possible to identify in the UAV DSM. These features are easily identifiable but there are other significant differences across the study area where the LiDAR model inundates further inland, namely, in the island formed south of the water reservoir, around the DEW-Line peninsula and the western shore near the airstrip. Overall, both elevation models show similar uppermost limits for the given flood scenario. The areas where the UAV DSM floods further inland are located primarily in the northern sector of the study area where the average distance from the LiDAR uppermost limit is less than 10 m. A 50-year return period (1,9 m above CD) storm surge results in a complete separation of Tuktoyaktuk and the DEW-Line peninsula from mainland even in 2020 if synchronized with a high late-summer tide. By 2100, for the scenario RCP8.5 (**Figure *8***), Flagpole Point becomes isolated, and another breakage is formed by Mangilaluk School, representing the most significant differences between the scenarios RCP4.5 and RCP8.5.

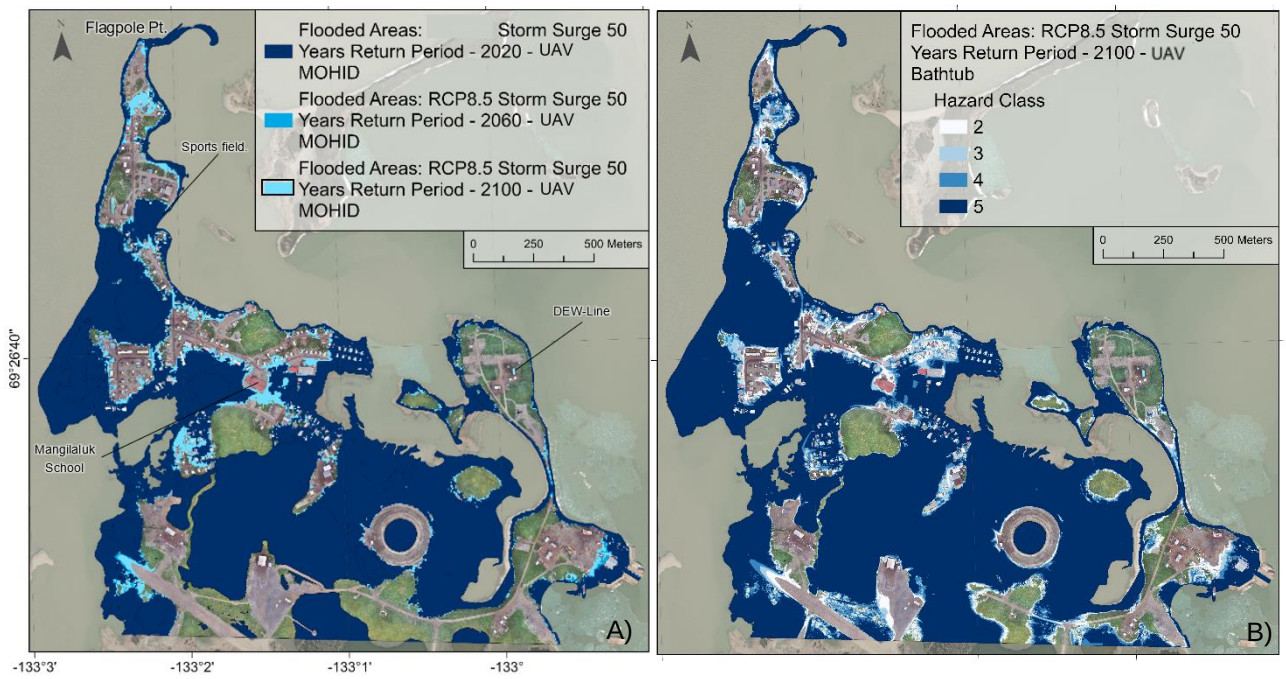

Figure 8. Predicted flooded extent for a 50-year return period storm surge on UAV DSM and scenario RCP8.5. A) MOHID. B) Bathtub model.

4.2.2. 100-year Return Period Storm Surge Event

The computed total area flooded in m² (**Figure 9**) regarding the 100-year return period storm surge and follows the same trend identified for the 50-year return period with LiDAR data returning larger flooded extents than the UAV and the bathtub model flooding more areas than MOHID. The results show that a 100-year return period storm, equivalent to 2,1 m above CD added to the MHAT, inundates 57,1% (UAV) and 65,8% (LiDAR) of the study area by using the bathtub model and 47,5% (UAV) and 52,3% (LiDAR) by MOHID. In 2060 all the percentages increase from 1 to 3% with the higher values corresponding to RCP8.5 scenario for the LiDAR simulations. For the year 2100, the bathtub model returns 80,7% (UAV) and 90,1% (LiDAR), while MOHID water surface covers 60 and 65% for the UAV and LiDAR, respectively.

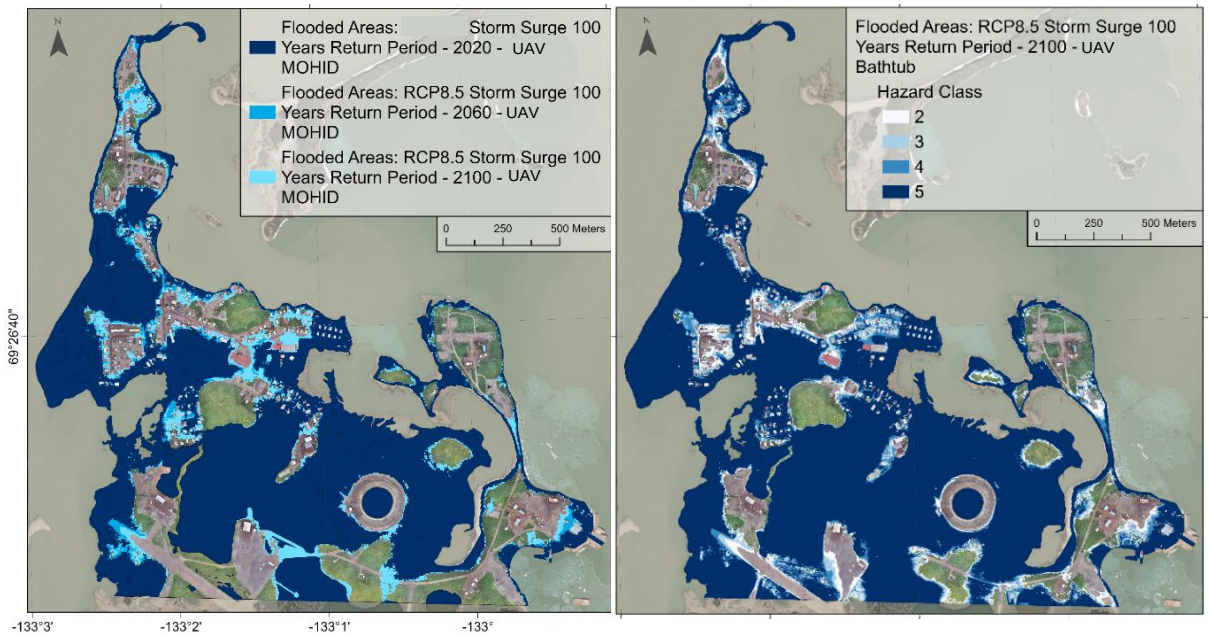

Figure 9. Predicted flooded extent for a 100-year return period storm surge in 2100 on UAV DSM and scenario RCP8.5. A) MOHID. B) Bathtub model.

5. Conclusion

The results obtained from this study show that with the methodology used it was possible to model and map with great accuracy the water surface changes in different scenarios in the Hamlet of Tuktoyaktuk. The models allowed the quantification and identification of flooded areas and to categorize the built environment by its vulnerability to sea level rise and storm surge events. The main goal of this thesis focused in developing a methodology that permitted the identification, with precision, of areas vulnerable to coastal flooding including two different sea level rise scenarios, for the years of 2060 and 2100, and extreme events with two different return periods. It was possible to conclude that the quality and availability of the data played a major role in flood mapping and that there is a significant water level data gap from 1982 to 1991 and 1992 to 2003 that can impact the results obtained by tidal harmonic analysis and extreme event analysis of storm surge levels. Regarding elevation data, using a UAV-derived well-georeferenced surface model with higher vertical and horizontal accuracy and spatial resolution, reduced significantly the overall uncertainty included in the bathtub model and, therefore, reduced over-estimation of flooded areas compared to LiDAR. The lower uncertainty of the UAV data drastically improved the water-surface modelling. With the tightening of areas with hazard classes of lower probabilities, the model showed precise overlaps of probability classes between 99.9% and 40% (classes 5 to 3) with the water surface captured by the drone footage, as well as by time-lapse cameras, used as ground truthing data. This reinforces the advantage of UAV over the available 2004 LiDAR data. Having an ultra-high-resolution mosaic of the study area revealed a major advantage to derive the local difference between vertical datums, to validate results by replicating the conditions registered at the time of the flight and identify details to a centimetric precision in 2D and 3D. Regarding the hydrodynamic modelling, the resampling from 0.1 x 0.1 m to 5 x 5 m cell size significantly reduced the vertical accuracy of the UAV model due to the interpolation algorithm. This transformation resulted in similar outputs for both LiDAR and UAV elevation datasets by diluting the differences. The culvert system had to be manually edited and exaggerated to be represented in 5 x 5 m cells after the smoothing effect of the algorithm. For a simplistic modelling of the water surface, the results show that complexity of the hydrodynamic model does not translate directly in a more accurate flood mapping. By maintaining the original cell size, the bathtub model does not loose vertical data and it offers the advantage of probabilistic mapping allowing the quantification of the flooded area and identification of the susceptibility by different hazard classes of specific locations. These drawbacks were also identified by Seenath et al. (2015) when comparing two different hydrodynamic models with a GIS-based bathtub approach.

Acknowledgments This work is part of the Nunataryuk funded under the European Union's Horizon 2020 Research and Innovation Programme under grant agreement no. 773421, and with co-funding by the Climate Change Preparedness in the North (CCPN) program.

References

1. Burn CR, Kokelj SV. (2009). The environment and permafrost of the Mackenzie Delta area. Permafrost and Periglacial Processes 20: 83 –105. https://doi.org/10.1002/ppp.655.
2. Burn, C.R., Zhang, Y. (2010). Sensitivity of active-layer development to winter conditions north of tree line, Mackenzie Delta area, western Arctic coast. In Proceedings 6th Canadian Permafrost Conference, 12–16 September 2010, Calgary, AB, Paper 194. Canadian Geotechnical Society; 1458–1465.
3. Fritz, M., Wetterich, S., Meyer, H., Schirrmeister, L., Lantuit, H., Pollard, W.H., 2011. Origin and characteristics ofmassive ground ice on Herschel Island (western Canadian Arc- tic) as revealed by stable water isotope and hydrochemical signatures. Permafr. Periglac. Process. 22:26–38. http://dx.doi.org/10.1002/ppp.714.
4. Harper, J.R., 1990. Morphology of the Canadian Beaufort Sea Coast. In: P.R. Hill (Editor), The Beaufort Sea Coastal Zone. Mar. Geol., 91 (Spec. Sect.): 75-91
5. Harper, J.R., Henry R.F., Stewart, G.G. (1988). Maximum storm surge elevations in the Tuktoyaktuk region of the Canadian Beaufort Sea. Arctic, 41(1), 48-52.
6. IPCC, (2021): Climate Change 2021: The Physical Science Basis. Contribution of Working Group I to the Sixth Assessment Report of the Intergovernmental Panel on Climate Change [Masson-Delmotte, V., P. Zhai, A. Pirani, S. L. Connors, C. Péan, S. Berger, N. Caud, Y. Chen, L. Goldfarb, M. I. Gomis, M. Huang, K. Leitzell, E. Lonnoy, J. B. R. Matthews, T. K. Maycock, T. Waterfield, O. Yelekçi, R. Yu and B. Zhou (eds.)]. Cambridge University Press. In Press.
7. Johannessen OM, Bengtsson L, Miles MW, Kuzmina SI, Semenov VA, Aleekseev GV, Nagurnyi AP, Zakharov VF, Bobylev L, Pettersson LH, Hasselmann K, Cattle HP (2002) Arctic climate change—observed and modelled temperature and sea ice vari- ability. Nansen Environmental and Remote Sensing Centre Tech Rep 218:22
8. Manson, G., and S. Solomon (2007): Past and future forcing of Beaufort Sea coastal change. Atmos.–Ocean, 45, 107–122.
9. NOAA (2021). Global mean sea level from TOPEX/Poseidon, Jason-1, Jason-2, and Jason-3. https://www.star.nesdis.noaa.gov/socd/lsa/SeaLevelRise/LSA_SLR_timeseries_global.php
10. Northwest Territories Bureau of Statistics (2021). Tuktoyaktuk Statistical Profile. https://www.statsnwt.ca/community-data/infrastructure/Tuktoyaktuk.html
11. Räisänen J. (2001) CO2-induced climate change in CMIP2 experiments: Quantification of agreement and role of internal variability. J Climate 14:2088–2104
12. Ramage, J. L., Irrgang, A. M., Morgenstern, A., & Lantuit, H. (2018). Increasing coastal slump activity impacts the release of sediment and organic carbon into the Arctic Ocean. Biogeosciences, 15(5), 1483–1495. https://doi.org/10.5194/bg-15-1483-2018
13. Solomon, S. M. (2005). Spatial and temporal variability of shoreline change in the Beaufort-Mackenzie region, northwest territories, Canada. Geo-Marine Letters, 25(2–3), 127–137. https://doi.org/10.1007/s00367-004-0194-x
14. Steedman AE, Lantz TC, Kokelj SV. (2016). Spatio-temporal variation in high-centre polygons and ice-wedge melt ponds, Tuktoyaktuk coastlands, Northwest Territories. Permafrost and Periglacial Processes (in press) https://doi.org/10.1002/ppp.1880
15. Timoney KP, La Roi GHL, Zoltai SC, Robinson AL. (1992). The high subarctic forest-tundra of northwestern Canada: position, width, and vegetation gradients in relation to climate. Arctic 45: 1 –19. https://doi.org/10.14430/arctic1367
16. Community of Tuktoyaktuk, Wildlife Management Advisory Council (N.W.T.), Tuktoyaktuk Conservation Plan Working Group. Joint Secretariat (2000), Tuktoyaktuk Community Conservation Plan: A plan for the conservation and management of renewable resources and lands within the Inuvialuit settlement region in the vicinity of Tuktoyaktuk, Northwest Territories.